Applied Catalysis B: Environmental 168-169 (2015) 183–194

Contents lists available at ScienceDirect

Applied Catalysis B: Environmental

journal homepage: www.elsevier.com/locate/apcatb

Limonene photocatalytic oxidation at ppb levels: Assessment of gas phase reaction intermediates and secondary organic aerosol heterogeneous formation

H. Ourrad, F. Thevenet*, V. Gaudion, V. Riffault

Mines Douai, SAGE, F-59508 Douai, France

ARTICLE INFO

Article history:
Received 6 August 2014
Received in revised form
19 November 2014
Accepted 24 November 2014
Available online 25 December 2014

Keywords:
Photocatalysis
Indoor air
Limonene
Secondary organic aerosols
Carbon mass balance

ABSTRACT

This study investigates the photocatalytic oxidation of limonene, used as a model terpenoid, close to indoor air conditions. Besides the characterization of limonene removal kinetic on the ppb range, special attention has been paid to reaction intermediates and by-products: (i) in the gas phase, (ii) in the adsorbed phase and (iii) in the particulate phase. All along the oxidation reaction organic reaction intermediates have been monitored. Despite a high conversion rate of limonene after 10 h of treatment, 20 primary and secondary reaction intermediates were detected and quantified in the gas phase with acetone and acetaldehyde as the most abundant ones. The characterization of limonene adsorbed on TiO_2 surface under UV illumination using DRIFTS pointed out the fact that the photocatalyst surface acts as a pool of heavy reaction intermediates, close to terpenoid structure, which may be responsible for the release of some secondary reaction intermediates. The mineralization of limonene has been assessed during the whole oxidation process through CO and CO_2 monitoring. CO_2 formation is observed more than 12 h beyond limonene complete removal, confirming the long term oxidation of the adsorbed phase. The photocatalytic heterogeneous formation of secondary organic aerosol is reported for the first time. A massive production of SOA since the first steps of limonene photocatalytic oxidation is evidenced. Based on the quantitative analyses performed, carbon mass balances have been calculated along the oxidation reaction advancement. The highest contributions of organic reaction intermediates and SOA in the carbon balance are respectively 12% and 1.6%. When limonene is removed from the gas phase, more than 60% of the carbon balance remains unidentified but this contribution can be mainly attributed to the adsorbed organic species. After 24 h of treatment, almost 75% of the organics are mineralized into CO_2.

1. Introduction

Indoor Air Quality (IAQ) has become a major public health issue due to the modern lifestyle increasing the time spent in indoor environments to more than 88% of the day in buildings (homes, offices) and 7% in transportation [1]. It is reported that a poor IAQ is generally correlated to the presence of a wide range of chemical pollutants, especially volatile organic compounds (VOCs) [2]. VOCs are the main pollutants found in indoor environments with concentrations generally higher than those found outdoors [3,4]. Over the last 20 years, the three main categories of VOCs identified in the buildings of European Union countries, are BTXS (benzene, toluene, xylene and styrene), terpenes (limonene, α-pinene) and carbonyl compounds (formaldehyde, acetaldehyde) [5]. These volatile compounds are emitted by a large number of sources like building materials, cleaning products, office equipments and combustion by-products. Human exposure to these VOCs induces a wide variety of symptoms related to Sick Building Syndrome (SBS) [6]. Moreover, the increasing number of respiratory diseases, allergies and asthma symptoms are clearly correlated to a poor indoor air quality [7].

Monoterpenes, whose chemical structures are based on the condensation of two molecules of isoprene (C_5H_8), are naturally emitted in the atmosphere by many plant species [8,9]. Besides, they are frequently observed in indoor environments [10]. D-Limonene, which is naturally present in citrus, mint and conifer essential oils, is recurrently measured in buildings at significant, but variable, concentrations. For instance, the maximum concentration (65 $\mu g\,m^{-3}$) recorded in the campaigns conducted by Schlink et al. [11] in three German cities is lower than the maximum value (159.4 $\mu g\,m^{-3}$) observed by Missia et al. [12] in various European

* Corresponding author. Tel.: +33 03 27 71 26 12.
E-mail address: frederic.thevenet@mines-douai.fr (F. Thevenet).

http://dx.doi.org/10.1016/j.apcatb.2014.11.048
0926-3373/

houses. When extensively used as a fragrance or a solvent [13,14], limonene concentrations may reach up to 1261 $\mu g\,m^{-3}$ as reported by Krol et al. [15]. Indoor concentrations of terpenes are highly dependent on human activities such as the use of air fresheners or cleaning products and air renewal rate. In addition to these artificial sources, limonene can also be emitted, to a lower extent, from wood-based furniture or materials [16]. Moreover, the limonene molecule presents two highly reactive double bonds (one endocyclic, one exocyclic) which may lead to the production of a variety of monocyclic oxygenated terpenoids which may be strongly irritating for skin and eyes [17,18]. Therefore, this compound was classified in the group 3 of the strategic document of the European Commission on air quality, which corresponds to chemicals requiring extensive research on human exposure and dose response [19].

Numerous studies have demonstrated that limonene ozonolysis leads to secondary organic aerosol (SOA) formation with high yields [20–23]. This homogeneous reaction between limonene and oxidants such as ozone is well described and reported [24,25]. In indoor environments, the significant occurrence of limonene makes possible the formation of ultrafine particles in the presence of ozone [26]. A recent study has pointed out SOA formation in schools during the use of a limonene-containing detergent [27]. In addition, Rossignol et al. [28] confirmed that the ozonolysis of limonene emitted from housecleaning products is responsible for SOA formation in real indoor environments. Recently, Waring et al. [29] showed that ozone reactions with limonene sorbed on various surfaces also contribute to the generation of SOA in indoor environments.

Photocatalytic oxidation (PCO) is an indoor air purification technique allowing VOC mineralization i.e. their transformation into CO_2 and H_2O. TiO_2 photocatalyst is currently used and implemented for the treatment of VOCs in indoor air due to its chemical stability, low cost and strong oxidizing potential under UV irradiation [30]. Few studies have investigated the photocatalytic oxidation of limonene. El Otmani [31] conducted a study on the photocatalytic degradation of limonene dissolved in acetonitrile. The author identified two main reaction intermediates: carvone and limonene oxide. In the treatment of liquid effluents produced by industrial activities related to essential oil extraction, Catanzaro et al. and Saverini et al. [32,33] evidenced the effectiveness of photocatalysis to remove a mixture of terpenes, including limonene, in aqueous synthetic solutions and collected wastewater, respectively. These two studies evidenced the potential action of TiO_2 photocatalyst on limonene structure; nevertheless, they are poorly related to indoor air specific issues. Regarding air treatment, the PhD thesis of Poncet-Vincent investigated the efficiency of photocatalytic oxidation to eliminate various VOCs including limonene [34]. Three photocatalytic materials were tested, leading to limonene mineralization rates between 70 and 90%. Using static and dynamic treatment systems, the author identified 40 reaction intermediates. However, these substances were not quantified and the study was performed with initial VOC concentrations of several hundreds of ppm, which are not representative of any typical indoor air conditions. More recently, limonene photocatalytic removal was investigated in the presence of ozone at lower levels, ranging from 0.5 to 9 ppm [35]. The authors highlighted the enhancement effect of ozone on the limonene photocatalytic degradation. Nevertheless, neither reaction intermediates nor SOA formation were investigated, whereas they are crucial issues regarding IAQ.

Considering the literature, D-limonene is sensitive to photocatalytic oxidation [34–37]; however, in the context of IAQ, we can wonder (i) what the gaseous side-products and the mineralization rate of limonene at ppb levels are, and (ii) whether the photocatalytic oxidation of a terpenoid under indoor air condition may lead to SOA formation.

In the present study, the photocatalytic oxidation of limonene was investigated in a 120 L Pyrex batch reactor at ppb levels to determine the kinetics of limonene removal under typical indoor air conditions. In particular, reaction intermediates, by-products and organic particles formed during the photocatalytic oxidation reaction were monitored and quantified. Finally, carbon mass balance calculations were performed to estimate the contribution of the various species along the oxidation reaction advancement.

2. Experimental

The main experimental setup is presented in Fig. 1. It is divided in four parts: (i) a VOC generation system, (ii) a 120 L Pyrex batch reactor, (iii) analytical systems dedicated to the gas-phase characterization at ppb levels, and (iv) analytical devices for the particulate phase characterization. This experimental setup has been built up in order to identify and quantify a wide range of species potentially formed in the gas and particulate phases along the oxidation reaction.

A complementary experimental setup based on a DRIFTS (Diffuse Reflectance Infrared Fourier Transform Spectroscopy) cell has been used in parallel for adsorbed phase characterization. For all experiments (gas phase and adsorbed phase), TiO_2 P25-Degussa was the photocatalyst used as received.

2.1. VOC generation system

A VOC generation system was developed in order to generate a controlled air flow containing limonene at targeted ppb level. "Zero-air" is generated by a purification system combining a Claind AZ-2020 zero air generator and a Pressure Swing Adsorption (PSA) device, which removes VOCs, CO_2 and moisture from ambient air leading to residual amounts of VOCs and CO_2 lower than 10 ppt and 10 ppb, respectively.

A 25 ppm calibrated gas cylinder of limonene balanced in nitrogen was supplied by PRAXAIR. Zero-air and gaseous limonene flows are regulated with appropriate ratios using Bronkhorst mass flow controllers (MFC) ranging from 0 to 4 L min^{-1} and from 0 to 50 mL min^{-1}, respectively. For all experiments, the concentration of limonene is set to 750 ± 20 ppb. The targeted concentration is obtained by diluting 15 mL min^{-1} of limonene in 485 mL min^{-1} of zero-air in the mixing chamber. Before each experiment, the gas mixture is directly sent to the TD-GC-FID/MS system, by by-passing the batch reactor, in order to check the limonene input concentration.

2.2. Reaction chamber

Photocatalytic experiments were carried out in a 120 L Pyrex chamber formerly developed and described by Debono et al. [38]. Briefly, this cylindrical reaction chamber is 935 mm high with an inner diameter of 470 mm. This large volume allows the sampling and analysis of the reaction chamber at each step of the reaction advancement. UV irradiation is obtained from nine PL-L-40 Phillips UV lamps emitting a broad band centered at 365 nm and without any emission below 350 nm. It was determined that the photon flux is homogeneous in the chamber with an average of 10 ± 1 mW cm^{-2} using a Solacheck spectro-radiometer in 70 different spots of the reaction chamber. The temperature is regulated at $23 \pm 1\,^{\circ}C$ using four fans located at the back of the UV insulating box. The photocatalyst powder (100 mg) is sieved on a circular Pyrex plate (positioned 5 cm above the bottom of the reactor) in order to ensure homogeneous dispersion of the material. Before each experiment, the chamber is purged with 50% humid air, under UV irradiation, for 12 h in order to clean the internal surface of the chamber and the

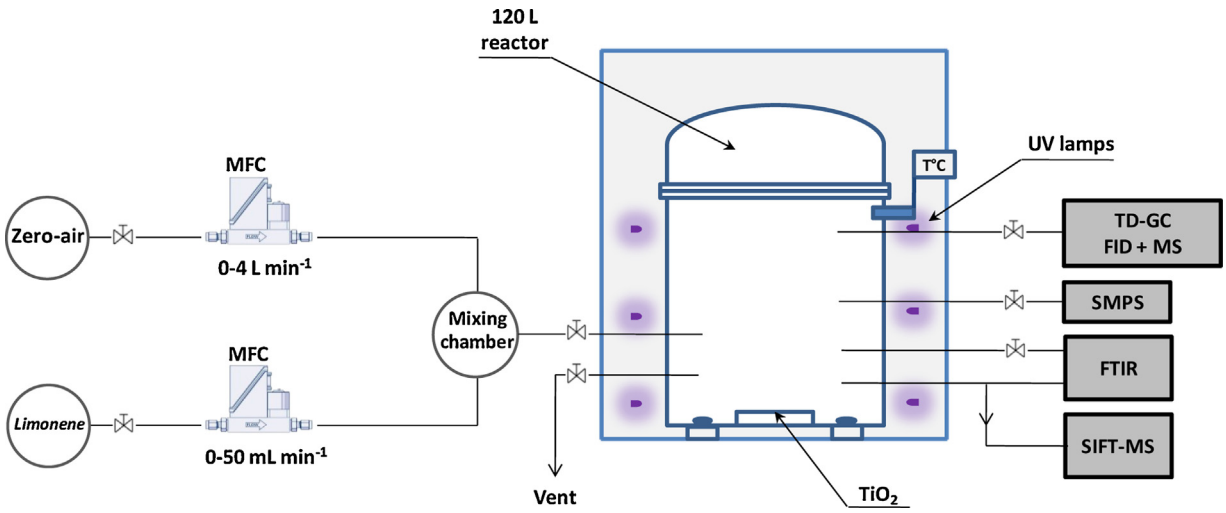

Fig. 1. General scheme of the experimental setup.

photocatalyst as efficiently implemented by Debono et al. [38]. This procedure ensures the reproducibility of the experiments.

All the experiments were performed under static and dry air conditions. In order to reach the adsorption equilibrium, in dark conditions, 750 ± 20 ppb of limonene at 500 mL min^{-1} total flow rate are sent into the chamber for 14 h. Then, the reaction chamber is closed. The chamber sealing has been evaluated through VOC static decay along 24 h and remains lower than 5% [38]. Before switching on the UV-irradiation, the initial concentration of limonene is measured twice. At $t = 0$ the UV-irradiation is started, then, the reaction chamber mixture is regularly monitored along the irradiation time in order to characterize the removal kinetics. Compared to dynamic flow reactors [36], the use of a batch reactor, or stirred tank reactor, to investigate VOC removal makes possible the characterization of the complete temporal decay, corresponding to the various advancements of the oxidation reaction. Thus, kinetic analysis of the experimental data is possible.

2.3. Gas phase analysis

The gas phase analysis is performed using mainly three different analytical devices: (i) Gas Chromatography (GC) coupled to MS and FID for VOC identification and quantification, (ii) derivatization and liquid Chromatography (HPLC) coupled to UV spectrometry for formaldehyde monitoring, and (iii) Fourier Transform Infrared (FTIR) spectroscopy for CO and CO_2 measurements.

For each VOC analysis by GC, 1 L of the gas mixture is collected online (Gerstel Thermo-Desorption System, TDS) from the chamber and pre-concentrated on a multi-sorbent cartridge (Carbopack X; Carbopack B; CarbopackC) at a constant flow rate of 100 mL min^{-1}. A maximum of 10 L, i.e. less than 10% of the total volume, is sampled in order not to modify significantly the reaction mixture inside the reaction chamber during the photocatalytic treatment. Therefore 10 analyses are performed during each experiment to determine the temporal profiles of limonene and reaction intermediates. After thermal desorption of the cartridge, the compounds are conducted by He used as carrier gas toward a cryogenic trapping capillary tube (Cooled Injection System, CIS), filled with Carbopack B, in order to refocus the analytes at −100 °C. The gas chromatographic analysis is carried out by a 6890 N/5975B type instrument from Agilent Technologies equipped with an Agilent DB-5MS chromatographic column (60 m × 0.32 mm × 1 μm). Samples are eluted using a thermal ramp of 15 °C min^{-1} from 0 to 250 °C. This column is connected to two different detectors using a calibrated Y-shaped restriction. Therefore, analytes are concurrently transferred to (i) a Flame Ionization Detector (FID), dedicated to compound quantification, and to (ii) a Mass Spectrometer (MS) dedicated to compound identification. The parameters of the TD-GC analytical system are summarized in Table 1.

The FID calibrations of the different intermediate compounds identified using the mass spectrometer and the NIST library (Mass spectral library NIST08) were performed in the ppb range. These substances were obtained from two different sources: (i) certified gas cylinders from Praxair, or (ii) vaporized liquid VOCs from Aldrich. The detection limits of each compound quantified in this study are listed in Table 2.

Formaldehyde is usually reported as a major by-product during the photocatalytic oxidation of VOCs, however, the above-mentioned GC analytical method is unable to detect this carbonyl species. Therefore, gas samples were collected online on Waters Silica cartridges impregnated with 2.4-dinitrophenylhydrazine (DNPH). The derivatization of formaldehyde is achieved at a flow rate of 100 mL min^{-1} for a total volume of 1 L and leads to the formation of a hydrazone which is eluted and analyzed by high performance liquid chromatography (Waters Alliance 2695) coupled with a UV detector (Waters 2487) as explained by Coddeville et al. [39]. The detection limit obtained for formaldehyde using this method is 10 ppb.

The detection and quantification of CO and CO_2 were carried out by a Fourier Transform Infrared (FTIR) spectrometer Antaris IGS. A

Table 1
Thermodesorption and gas chromatography parameters.

Thermodesorption system	
Initial temperature (°C)	10
Temperature ramp (°C min^{-1})	50
Final temperature (°C)	250
Final time (min)	10
Flow rate (mL min^{-1})	50
Refocusing on CIS and injection into GC	
Initial temperature (°C)	−100
Temperature ramp (°C s^{-1})	12
Final temperature (°C)	250
Final time (min)	10
Gas Chromatographic system	
Initial temperature (°C)	0
Initial time (min)	4
Temperature ramp (°C min^{-1})	15
Final temperature (°C)	250
Flow rate (mL min^{-1})	4

Table 2
List of the compounds identified in the gas phase during the 750 ppb limonene photocatalytic degradation under dry air on TiO_2, with their detection limits expressed in ppt. (M.V.K. = methyl vinyl ketone).

Aldehydes	D.L. (ppt)	Ketones	D.L. (ppt)	Terpenoids	D.L. (ppt)	Caroxylic acids	D.L. (ppt)	Alcohols	D.L. (ppt)	Others	D.L. (ppt)
Acetaldehyde	43	Acetone	15	D-carvone	5	Acetic	20	1-Butanol	13	T.M.P.	3
Heptanal	7	M.V.K.	7	L-carvone	5	Pentanoic	6	Ethanol	14	Methyl acetate	6
Methacrolein	29	2-butanone	5	Carvomenthenal	7					CO	76×10^3
2,3-Dihydrofurane	12	2-pentanone	17							CO_2	10×10^3
Butanal	8										
Pentanal	9										
Formaldehyde	10×10^3										

heated 10 m optical-path cell coupled with a liquid nitrogen cooled MCT (Mercury Cadmium Telluride) detector is used. FTIR spectra are collected using Result-3 software with 6 scans per spectrum and a spectral resolution of 0.5 cm^{-1}. CO_2 quantification is obtained by integrating peaks in the 2388–2383 cm^{-1} infrared region associated to the CO_2 fundamental asymmetric stretch vibration. In order to avoid the overlapping signals of CO with H_2O, the quantification of CO is performed using the average of four rotational absorption peaks corresponding to the C—O stretch vibration: R(4), R(5), R(6) and R(7)peaks at 2163.5–2160.1 cm^{-1}, 2167.4–2163.7 cm^{-1}, 2170.7–2167.1 cm^{-1} and 2173.1–2171.9 cm^{-1}, respectively. CO_2 and CO were calibrated by passing 1 L min^{-1} of these standard gases provided by Praxair through the gas cell. Calibration concentrations were adjusted from 240 ppbv to 10 ppmv. Detection limits are respectively determined as 10 ppbv and 76 ppbv for CO_2 and CO. These values are calculated as three times the signal-to-noise ratio in the regions of interest.

Additionally, for experiments focusing on aerosol formation for which a higher time resolution was needed the limonene concentration was monitored using a selected ion flow tube mass spectrometer (SIFT-MS) Voice 200. SIFT-MS is based on the chemical ionization of a molecule using precursors (H_3O^+, NO^+ and O_2^+) during a defined time, typically in milliseconds (ms). 30 mL min^{-1} were continuously sampled at the reactor outlet during the first 4 h of irradiation. The detection limit of limonene by SIFT-MS is 50 ppb.

2.4. Adsorbed phase characterization

The in situ monitoring of the photocatalyst surface has been performed directly in a DRIFT cell (Harrick, Praying Mantis) coupled with a FTIR spectrometer (Nicolet 6700). The inlet of the cell is connected to the VOC generation system. A 20 mg bed of TiO_2 particles is placed on the grid inside the DRIFT cell. This configuration allows a constant gas flow through the catalyst bed. Two ellipsoidal mirrors focus the infrared beam at the upper part of the catalyst bed and collect the scattered light to the MCT detector. UV irradiation of TiO_2 is performed from the outer part of the DRIFT cell, at a distance of 3 cm from the catalyst bed. UV-LEDs are used to irradiate the photocatalyst surface with a photon flux of 2.5 mW cm^{-2}. The emission spectrum of the UV-LEDs is centered at 365 nm. DRIFTS spectra are recorded using Omnic software with 16 scans per spectrum and a spectral resolution of 4 cm^{-1}.

Prior to any photocatalytic experiments, the catalyst is thermally pretreated at 400 °C for 1 h under zero air flow (250 mL min^{-1}) in order to clean the surface and ensure reproducibility. After thermal pretreatment, a reference spectrum with 500 scans is recorded at room temperature. Then the cell is swept with 5 ppm of limonene diluted in air under a 250 mL min^{-1} air flow. Under these conditions, the adsorption equilibrium of limonene can be monitored by DRIFTS. The equilibrium is reached within about 1 h of adsorption. Before UV irradiation, the cell is thoroughly flushed under zero air for about 2 h in order to remove the reversibly adsorbed fraction of limonene. Finally, UV irradiation is performed under zero air flow and the evolution of the adsorbed phase is followed by DRIFTS.

2.5. Particulate phase analysis

Particle size data are collected every 4 min over 44 channels in the range 5.5–350.4 nm using a Scanning Mobility Particle Sizer (SMPS) Grimm 5403. The SMPS consists of a Condensation Particle Counter (CPC) coupled with a Diffusion Mobility Analyzer (DMA). Aerosols are sampled at a flow rate of 300 mL min^{-1}, through a ¼" stainless steel tubing placed 10 cm above the photocatalyst bed. The residence time of the particles in the tube was estimated to be 1.6 s. In order to keep the overall reactor volume (hence the pressure) constant, experiments are performed in a dynamic state where zero air is added in the reactor to compensate for each sample taken. Dilution was taken into account as explained in Section 3.

3. Results and discussion

3.1. Limonene removal kinetics

An example of a decay profile of D-limonene as a function of irradiation time is reported as an inset in Fig. 2. In order to describe the evolution of the D-limonene degradation rate, Eq. (1) can be used.

$$r = k \cdot C_1^{n_1} \cdot C_2^{n_2} \quad (1)$$

In Eq. (1), r is the compound removal rate as a function of reactant concentrations C_1 and C_2; k is the reaction rate constant, n_1 and n_2 are the partial reaction orders regarding each reactant. During the photocatalytic oxidation reaction, limonene reacts either with photogenerated holes or with hydroxyl and superoxide radicals formed on the surface of the photocatalyst. Considering a steady-state approximation for these reactants, which is all the more valid

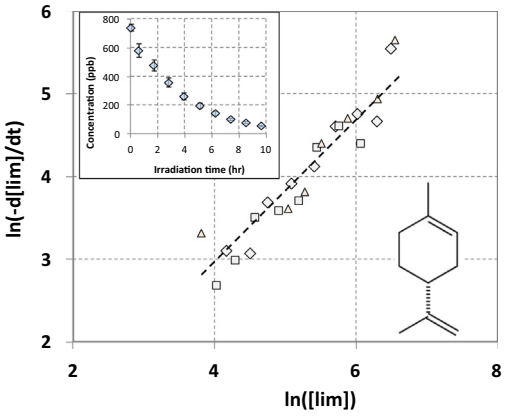

Fig. 2. Evolution of ln(−d[lim]/dt) as a function of ln([lim]) obtained from three photocatalytic degradations of limonene on TiO_2 under dry air with 750 ppb initial concentration. Inset: example of a temporal profile of limonene photocatalytic oxidation.

Table 3
List of the primary (a) and secondary (b) reaction intermediates identified and quantified in the gas phase during the photocatalytic oxidation of 750 ppb of limonene under dry air; "t_{Cmax}" indicates the maximum of the temporal profiles, and "t_{delay}" indicates the initial formation time of the secondary intermediates. (M.V.K. = Methyl Vinyl Ketone; T.M.P. = 2,4,4-trimethyl-1-pentene).

(a)

Aldehydes	Formula	t_{Cmax} (h)	Ketones	Formula	t_{Cmax} (h)	Terpenoids	Formula	t_{Cmax} (h)
Acetaldehyde	C_2H_4O	2.7	Acetone	C_3H_6O	1.6	D-Carvone	$C_{10}H_{14}O$	7.3
Heptanal	$C_7H_{14}O$	5	M.V.K.	C_4H_6O	5	L-Carvone	$C_{10}H_{14}O$	6.2
Methacrolein	C_4H_6O	5	2-Butanone	C_4H_8O	5	Carvomenthenal	$C_{10}H_{16}O$	2.7
2,3-Dihydrofurane	C_4H6O	5						
Butanal	C_4H_8O	6.2						
Pentanal	$C_5H_{10}O$	7.3						
Formaldehyde	CH_2O	6.2						

(b)

Carboxylic acids	Formula	t_{delay} (h)	t_{Cmax} (h)	Alcohols	Formula	t_{delay} (h)	t_{Cmax} (h)
Acetic acid	$C_2H_4O_2$	0.5	7.3	1-butanol	$C_4H_{10}O$	0.5	6.2
Pentanoic acid	$C_5H_{10}O_2$	1.6	7.3	Ethanol	C_2H_6O	1.6	5

Terpenoids	Formula	t_{delay} (h)	t_{Cmax} (h)
T.M.P.	C_8H_{16}	0.5	6.2
Methyl acetate	C_3H_6O	0.5	7.3
2-Pentanone	$C_5H_{10}O$	1.6	6.2

since limonene initial concentration is in the ppb range, Eq. (1) can be simplified as follows:

$$r = -\frac{d[lim]}{dt} = k_{app} \cdot [lim]^n \quad (2)$$

In Eq. (2), [lim] represents the concentration of D-limonene, k_{app} is the pseudo reaction constant, n is the pseudo order of the reaction and t the irradiation time. Eq. (3) results from the linearization of Eq. (2).

$$\ln \frac{-d[lim]}{dt} = n \cdot \ln \cdot([lim]) + \ln(k_{app}) \quad (3)$$

It is then possible to evaluate k_{app} and n from the linear regression of experimental data. Under our experimental conditions, a linear relationship is confirmed by plotting $\ln(-d[lim]/dt)$ as a function of $\ln([lim])$ for three different experiments (Fig. 2). It makes possible the evaluation of k_{app}, from the intercept at the origin, and n, from the slope of the linear regression fit. The value of n was found to be equal to 1.04 ± 0.06. Thus, the limonene photocatalytic removal can be described by a mono-exponential decay corresponding to a pseudo first-order kinetic. In addition, the average value of k_{app} was calculated as $0.23 \pm 0.04\ h^{-1}$. These findings evidence that limonene decay profiles are consistent with the results observed for other classes of VOCs such as toluene [38] and decane [40], close to real indoor air treatment conditions.

3.2. Reaction products

3.2.1. Characterization of gas phase organic reaction intermediates

During the limonene photocatalytic degradation, a total of 20 VOCs have been identified and quantified in the gas phase. As reported in Table 3, the majority of the reaction intermediates are non-cyclic oxygenated VOCs. In contrast, the study of Poncet-Vincent [34] clearly highlighted the predominance of 8 different terpenoids among the reaction intermediates during the photocatalytic degradation of limonene, with an initial concentration exceeding 600 ppm. However, in this study, only 3 carvones are identified and quantified. This difference can be ascribed to the fact that, in the study of Poncet-Vincent [34], the reaction was performed at high concentrations, promoting a high surface coverage of the catalyst, which may favor the subsequent release of intermediates in the gas phase. The influence of the photocatalyst surface coverage on reaction intermediate release in the gas phase has been previously pointed out by Thevenet et al. [41]. In our study performed at ppb levels, we suggest that most of the heaviest and partially oxidized reaction intermediates, especially terpenoids, remain adsorbed on the photocatalyst surface. This point is addressed in more details in Section 3.2.2 by DRIFTS experiments.

The temporal profiles of the reaction intermediates are determined throughout the degradation of limonene. Two types of temporal profiles are observed in this study:

(i) primary intermediates which are characterized by an initial formation rate different from zero at $t = 0$,
(ii) secondary intermediates which are characterized by an initial formation rate equal to zero from $t = 0$ up to a defined reaction time so called "delay time" and noted t_{delay} in Table 3.

For each reaction intermediate, the time for which the maximum concentration was reached (t_{Cmax}) is listed in Table 3.

The temporal evolutions of the primary intermediates are reported in Fig. 3. All terpenoids are characterized by the same initial formation rate on the first 2 h of experiments. However, it can be noticed that their maximum concentrations are not reached at the same time in all three cases; they range between 3 and 6 h of irradiation. These three reaction intermediates retain the terpenoid structure of D-limonene. Carvones were also identified in former studies conducted in the liquid [31,42,43] and gas phases [34]. D- and L-Carvones result from the self-oxidation of limonene [44] while carvomenthenal comes from an addition on the exocyclic double bond. It is reported in the literature that limonene oxidation products, such as carvones, are clinical allergens [45,46]. For instance, allergenic effects on guinea-pigs are observed during prolonged air exposure, for at least 2 months [47]. In this study, the total amount of carvones quantified in the gas phase remains lower than 0.8 ppb and limited in time. Thus, the risk of sensitization during the photocatalytic treatment of limonene at ppb level should not be significant.

Primary intermediates other than carvones do not contain any cyclic structure (Fig. 3b–d), suggesting they originate from the ring-opening of limonene or terpenoid intermediates. As shown in Fig. 3b–d, carbonyls are the major gas phase reaction intermediates

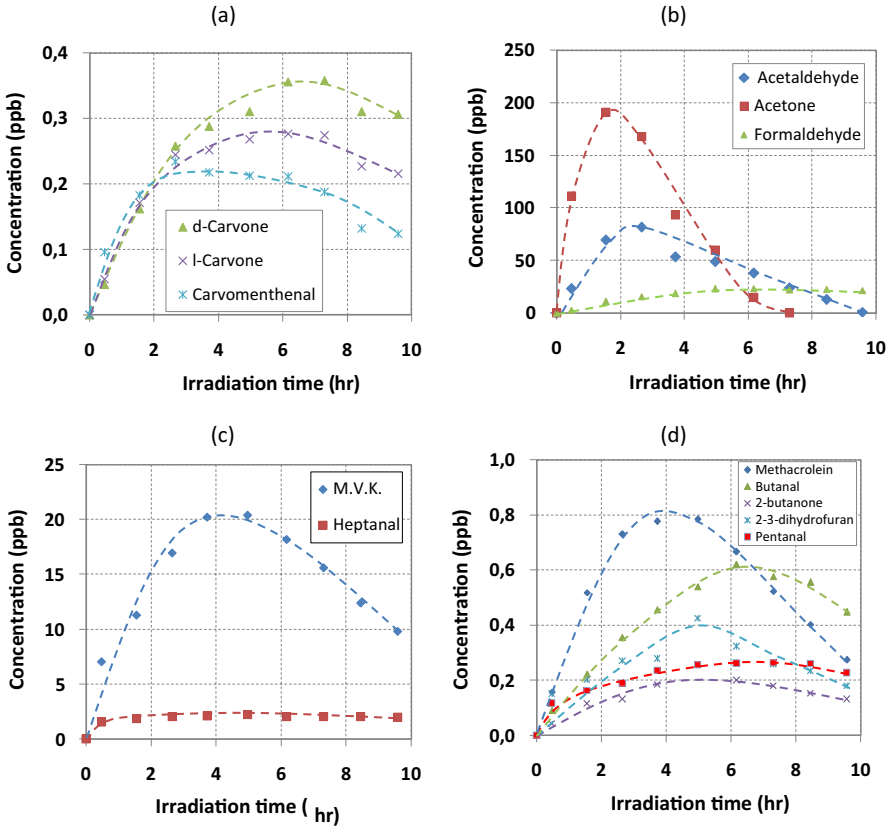

Fig. 3. Temporal profiles of the primary reaction intermediates during the photocatalytic oxidation of 750 ppb of limonene on TiO_2 under dry conditions. (M.V.K. = Methyl Vinyl Ketone).

in terms of variety and concentration. Unexpectedly, formaldehyde is not quantified as the most abundant intermediate. Acetaldehyde and acetone can be considered as the main gaseous intermediates regarding their concentrations, with maximum respective concentrations of 82 and 190 ppb, after only 3 h of irradiation. Furthermore, they disappear from the gas phase simultaneously with the removal of limonene, whereas other carbonyl species, and especially formaldehyde, remain in the gas phase. This behavior suggests that acetaldehyde and acetone directly originate from the degradation of gas phase limonene. The maximum concentrations of primary intermediates containing between 4 and 5 carbon atoms (methacrolein, butanal, 2-butanone, 2–3 dihydrofuran, pentanal) are reached after 4 h of irradiation. They can be derived from the degradation of limonene or from the oxidation of intermediate compounds present in the adsorbed phase.

The temporal profiles reported in Fig. 4a–c correspond to secondary reaction intermediates. These compounds are detected in the reaction chamber beyond 0.5 and 1.5 h of irradiation. In previous articles from our group [38,40] dealing with the toluene and decane photocatalytic degradations at ppb levels and using the same reactor and analytical devices, no secondary intermediates were identified, all detected substances being formed from $t = 0$. The formation of secondary reaction intermediates requires the achievement of first reaction steps. Some of the secondary reaction intermediates, such as acetic acid, methyl acetate and ethanol, are characterized by low molecular weights and t_{Cmax} values from 5 to 7 h. This suggests that they originate from the subsequent oxidation of gas phase primary intermediates. However, other secondary intermediates, such as trimethyl-1-pentene, pentanoic acid and 2-pentanone, contain between 5 and 8 carbon atoms. Their maximum concentrations are relatively high, from 5 to 50 ppb, and they are observed between 6 and 8 h of irradiation. Such characteristics suggest that these species may mainly originate from the oxidation of heavy reaction intermediates adsorbed on the photocatalyst surface. This hypothesis is discussed while evaluating the photocatalytic reactivity of the adsorbed phase in the following section.

3.2.2. *Adsorbed phase characterization*

Considering the low amount of terpenoid compounds monitored in the gas phase and the formation of secondary intermediates containing more than 5 carbon atoms beyond 6 h of irradiation, complementary experiments were carried out to investigate the photocatalyst adsorbed phase. These experiments have been performed using a DRIFT cell in order to investigate: (i) the adsorption of limonene on TiO_2 and (ii) the fate of adsorbed species under UV irradiation. The adsorption of limonene on TiO_2 leads to the appearance of typical absorption bands at 2974, 2923 and 2875 cm^{-1} associated to the C—H stretch vibration of methyl groups (Table 4). More precisely, the band at 2923 cm^{-1} has been used to follow limonene adsorption, desorption and conversion on TiO_2. The experiment was divided into three steps: (i) 5 ppm limonene diluted in air are sent into the DRIFTS cell on the surface of TiO_2, and limonene adsorption is monitored, (ii) the DRIFTS cell is flushed with zero air to remove the reversibly adsorbed limonene, (iii) the photocatalyst surface is illuminated with UV-LEDs.

Fig. 5 reports the evolution of the band at 2923 cm^{-1}, corresponding to limonene, along the three experimental steps. During the adsorption step, the saturation of the band is observed within 1.1 hour, confirming the complete coverage of limonene adsorption sites on TiO_2 surface. Beyond 1.1 h, the flushing step induces a steep decrease in the amount of adsorbed limonene corresponding to the

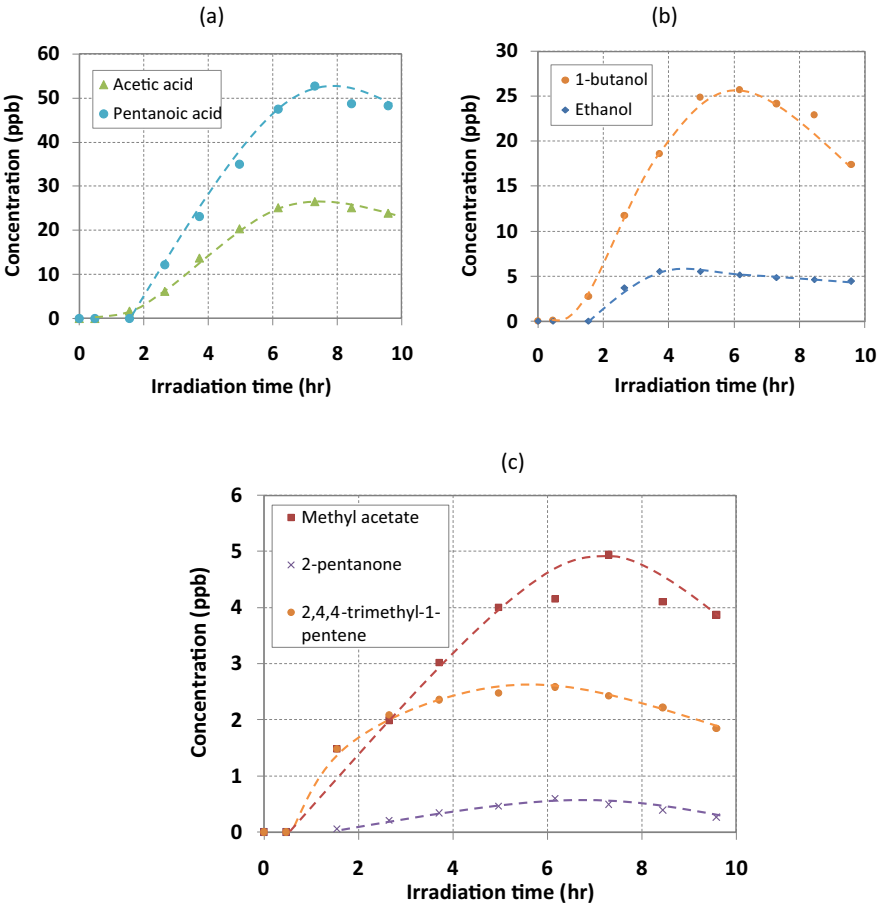

Fig. 4. Temporal profiles of the secondary reaction intermediates during the photocatalytic oxidation of 750 ppb of limonene on TiO_2 under dry conditions.

Table 4
Assignment of vibrational wavenumbers monitored by DRIFTS during the photocatalytic oxidation of limonene adsorbed on TiO_2 and comparison with literature data.

Adsorbed compounds	Vibration mode	Wavenumber (cm^{-1})	
		This work (position of the maximum)	References (range of wavenumbers)
Limonene	ν_{C-H}	2974, 2923, 2875	3000–2800 [37]
Carbonyle	$\nu_{C=O}$	1685	1729–1686 [48]
Formate	$\nu_{s\ COO}$	1360	1360 [49]
Formate	$\nu_{as\ COO}$	1559	1554 [49]
Alkene	$\nu_{C=C}$	1624	1680–1600 [50]

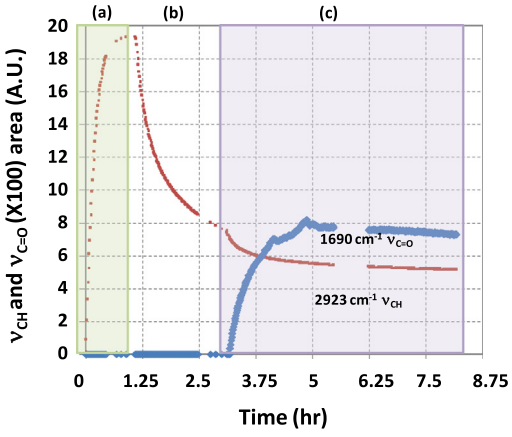

Fig. 5. DRIFTS temporal evolutions of the band at 2923 cm^{-1} corresponding to ν_{CH} from adsorbed limonene, and the band at 1690 cm^{-1} corresponding to $\nu_{C=O}$ from adsorbed carbonyl compounds, during (a) the adsorption of limonene, (b) the flushing under zero air and (c) the UV illumination on TiO_2 surface.

desorption of reversibly adsorbed, i.e. physisorbed, limonene from TiO_2 surface. Then, the band at 2923 cm^{-1} tends to stabilize, indicating that TiO_2 surface is mainly covered by irreversibly adsorbed limonene.

UV illumination is switched on after 3.2 h. As soon as illumination starts, two main phenomena can be observed in Fig. 5. First, the band at 2923 cm^{-1} corresponding to limonene ν_{CH} decreases, meanwhile, the band at 1690 cm^{-1} corresponding to $\nu_{C=O}$ for adsorbed carbonyl compounds increases. The apparition of the band at 1690 cm^{-1} simultaneously with UV illumination is evidence of the adsorbed phase oxidation of limonene. Moreover, UV irradiation also induced the apparition of absorption bands attributed to formates and alkenes, confirming the oxidative conversion of limonene. Absorption bands for formates and alkenes are intense enough to be clearly identified, but remain too weak to accurately plot their temporal evolutions. The characteristic wavenumbers of the compounds identified in the adsorbed phase are summarized in Table 4 [48–50]. The formation of such adsorbed species, especially surface carbonyl compounds, was evidenced

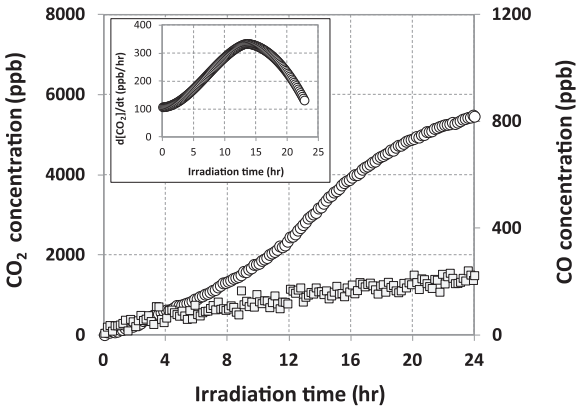

Fig. 6. Temporal evolutions of CO and CO_2 concentrations during the photocatalytic oxidation of 750 ppb of limonene under dry conditions. Open circles: CO_2; open squares: CO. Inset: evolution of CO_2 formation rate (ppb h^{-1}) calculated from CO_2 temporal profile.

in previous studies. Kibanova et al. [37], using Attenuated Total Reflection Fourier Transformed Infrared Spectroscopy (ATR-FTIR), reported the formation of adsorbed species containing vibration modes of carbonyl and carboxylate groups resulting from the limonene photocatalytic oxidation, which is consistent with our observations. Similarly, Salem et al. [51] investigated the photocatalytic removal of a mixture of terpenes including limonene and identified carbonyls, carboxylic acids and cyclic ketones as adsorbed intermediates using DRIFT spectroscopy.

The decrease in the ν_{CH} band at 2923 cm^{-1} indicates the consumption of adsorbed limonene molecules by photocatalytic processes. More precisely, the appearance of ν_{sCOO} and ν_{asCOO} corresponding to formate and $\nu_{C=O}$ corresponding to carbonyls confirms that adsorbed limonene molecules are oxidized. In the carboxylate corresponding wavenumber range, several peaks can be seen and most of them overlap. Only the vibrational contribution of formates has clearly been evidenced. The presence of other carboxylates cannot be excluded; however it was not possible to assess their identification under our experimental conditions. The relatively weak decrease in the ν_{CH} band at 2923 cm^{-1} (only 25% after 2 h of irradiation) suggests that most of the reacted limonene remains in the adsorbed phase. As suggested in Section 3.2.1, the hypothesis of partially oxidized terpenoids accumulated on TiO_2 is strengthened. As a result, the adsorbed phase could be considered as a pool of terpenoid compounds which may (i) lead to the release of various reaction intermediates and (ii) be gradually mineralized along the photocatalytic reaction.

3.2.3. Mineralization: CO and CO_2 formation

In spite of the fact that limonene is removed from the gas phase within approximately 12 h, the formation of CO and CO_2 was monitored during 24 h in order to investigate the mineralization process beyond limonene removal. Temporal profiles for CO and CO_2 are reported in Fig. 6.

The concentrations of CO and CO_2 in the batch reactor continuously increased along the 24-h experiment. CO and CO_2 are produced from the first oxidation steps since their initial formation rates at $t = 0$ are respectively 30 and 110 ppb h^{-1}. It can be seen in Fig. 6 that the formation of CO_2 is clearly favored compared to CO formation; after 24 h, the concentration of CO_2 exceeds the concentration of CO by a factor of 24. The continuous increase of CO and CO_2 along the experiment evidences that organic matter is mineralized during the photocatalytic removal of limonene and far beyond.

As shown in Fig. 6, the CO_2 temporal profile is characterized by a sigmoidal shape indicating that the CO_2 formation rate varies along the photocatalytic process. To assess this point, their evolution has been calculated as a function of irradiation time and reported in Fig. 6, where their variation can be divided in two parts. First, a significant increase is noticed from 0 to 14 h of illumination; on that time interval, the CO_2 formation rate reaches a maximum value of 340 ppb hr^{-1}. Second, a substantial decline of the CO_2 formation rates is observed beyond 14 h. This behavior can be correlated to the evolution of organic species to be oxidized in the batch reactor. Indeed, CO_2 production is directly impacted by the structure and the oxidation state of the VOCs to be treated, i.e. the number of elementary steps to produce CO_2. From 0 to 14 h, the increase in the CO_2 formation rate can be related to the advancement of the organic compound oxidation state with time. This point is supported by the nature and the temporal profiles of reaction intermediates in the gas and adsorbed phases. The opening of the terpenoid ring and the shortening of the carbon chain both promote mineralization rate. Indeed, comparing the conversion of 17 different VOCs, Alberici and Jardim [52] evidenced the lowest conversions for aromatic compounds and the highest ones for light, linear and oxidized VOCs. Similar trends in CO_2 production rates were reported by Debono et al. [38] during the investigation of toluene photocatalytic mineralization at ppb level in a batch reactor. However, the evolution of CO_2 formation rate was completely different in the case of decane photocatalytic oxidation which confirms the correlation between structure and mineralization kinetics [40]. Beyond 14 h, the decline in the CO_2 formation rate can be correlated to the gradual depletion of organic reaction intermediates from both the gas and adsorbed phases. It is important to note that in spite of limonene removal from the reactor after 10 h of treatment, the mineralization process still goes on; in particular, CO_2 concentration reaches 5490 ppb after 24-h illumination, corresponding to 74% of the reaction carbon mass balance. Conversion of the gas phase and also adsorbed phase reaction intermediate is a key step in the mineralization process.

3.2.4. SOA formation

The homogeneous reactions between limonene and oxidants such as ozone lead to the formation of both gaseous [53] and particulate products [21]. Limonene photocatalytic oxidation produces a wide variety of gaseous intermediates during the first hours of treatment, among which many of them such as terpenoids and carboxylic acids have vapor pressures low enough to partition between the gas and particulate phases during the heterogeneous oxidation of limonene and thus to contribute to SOA formation. Indeed, particles have been observed during the photocatalytic oxidation of 750 ppb limonene.

Before switching on the UV lamps, no particles were observed in the photocatalytic chamber. In the CPC mode, SOA formation was detected after 6 min of irradiation, indicating that their production requires the presence of precursor compounds in the gas phase. Fig. 7 presents the number size distribution obtained by connecting the DMA upstream the CPC (cf. §2.5) and sampling the batch reactor mixture about every 5 min during the first 45 min after irradiation then every half hour up to 8 h. The temporal profiles show a unimodal distribution whatever the time with a particle modal diameter shifting from 51.5 nm after 10 min to about 80 nm when the maximum number concentration is reached (i.e. at 24 min of irradiation) and further to 192 nm after 8 h of irradiation. The number decrease and average size increase is expected, due to particle coagulation or condensation onto preexisting aerosols for ultrafine particles and semi-volatile vapors to form larger particles at higher irradiation times.

The SOA mass concentration could be calculated from SMPS size distributions assuming spherical particles with a density of 1.25 g cm^{-3} [54,55]. Due to the regular addition of known amounts of zero air (for a total of about 30 L) in order to keep the reactor at atmospheric pressure despite sampling, a dilution effect had to

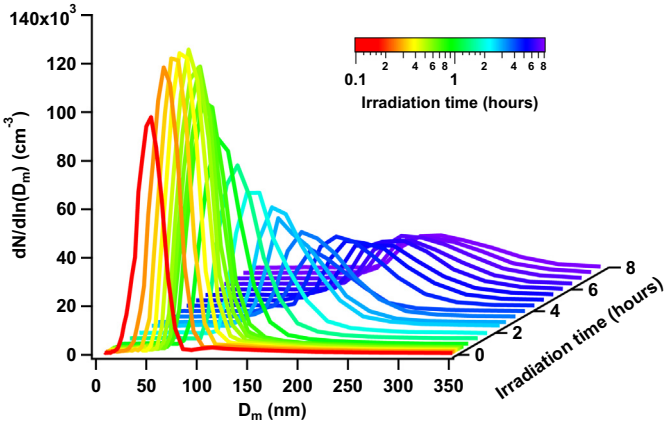

Fig. 7. Evolution of the SOA number size distribution during the photocatalytic oxidation of 750 ppb of limonene under dry conditions (t = 0 corresponds to the beginning of UV irradiation).

be taken into account. The dilution factor was calculated at each sampling point and ranged between 1 and 24% for 10 min and 8 h of irradiation, respectively. Fig. 8 shows the aerosol mass concentration before and after correction for the dilution effect. Aerosol wall losses in the reactor were estimated using a method previously developed and used in other studies [56,57], in which the loss rate is assumed to be first order and independent of the particle size. Only data points after the formation of new particles had stopped, i.e. after 5 h of irradiation were taken into account. The rate constant, k_{loss}, could be derived from Eq. (4):

$$\ln \mathrm{M}(t) = -k_{\mathrm{loss}} \cdot t + \mathrm{C} \quad (4)$$

where M(t) is the aerosol mass concentration measured at time t and corrected for dilution, and C a constant. The slope of the linear fit led to a value of k_{loss} = 0.046 hr^{-1}, similar to previously reported values [56,58]. Wall loss and dilution corrections were applied to the experimental data as illustrated in Fig. 8. The overall corrections were less than 15% until 1 h of irradiation but reached up to 70% for the last experimental point, mostly due to wall loss corrections.

SOA formation is a complex process, involving the gas-particle conversion of oxidized VOCs. In order to better assess the chemical mechanisms during the partitioning of semi-volatile hydrocarbons between the gas and particle phases, the SOA time-dependent

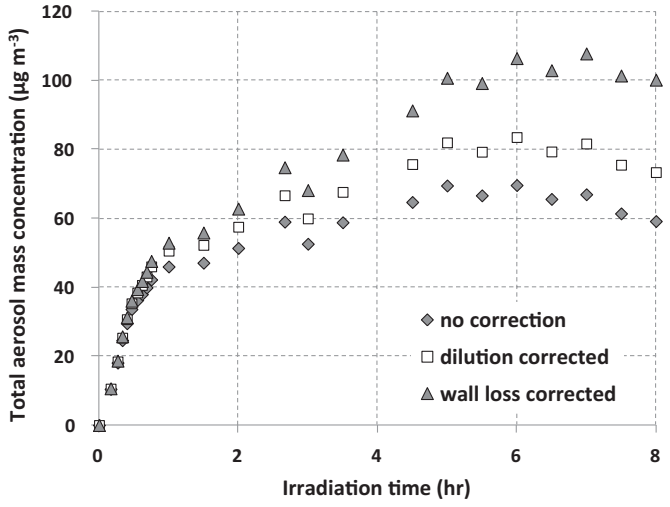

Fig. 8. Aerosol mass concentrations measured during the photocatalytic oxidation of 750 ppb of limonene under dry conditions as a function of irradiation time, after taking into account dilution effects and wall losses in the reactor.

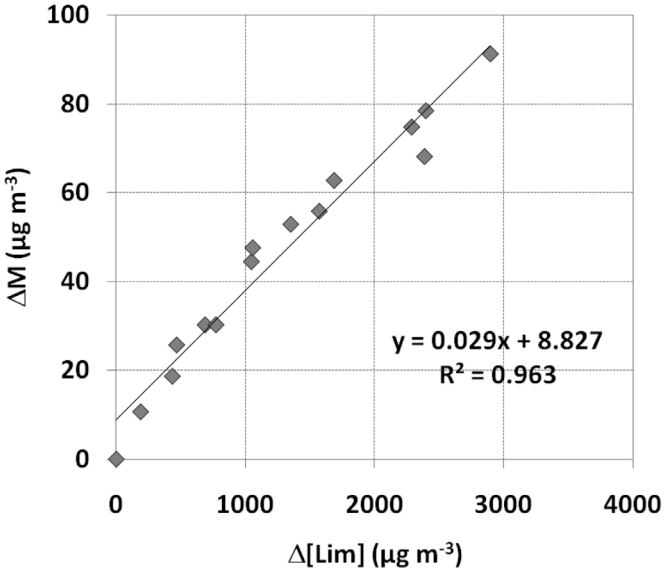

Fig. 9. Time-dependent growth curve of ultrafine particles detected during the photocatalytic oxidation of 750 ppb of limonene under dry conditions.

growth curve is modeled by plotting the aerosol mass formed (ΔM) as a function of the amount of limonene reacted (Δ[Lim]) during the first 4 h of irradiation of a specific experiment, during which the limonene concentration was determined with a high-time resolution by SIFT-MS measurements. Fig. 9 shows the SOA time-dependent growth data observed during limonene photocatalysis under dry conditions. The aerosol mass increases linearly till the consumption of ca. 70% of limonene after 4 h of irradiation. The linearity of the aerosol growth curve has been observed in many previous studies (e.g. Ng et al. [55], Coeur-Tourneur et al. [58]). Due to the lack of limonene concentration values at longer reaction times and since it was not entirely consumed after 4 h, we could not confirm previous findings from Ng et al. [55] who observed that limonene growth curves (like other terpenoids with more than one double bond) showed a typical behavior when oxidized by OH or ozone, with aerosols still formed after the terpene had been entirely consumed. They suggested that for this type of species, SOA formation is not only due to a rate-limiting step linked to the first-generation products, but that secondary products resulting from their further oxidation are rate-determining as well. In our case, the aerosol total mass concentration seems to stabilize in the reactor after 5 h of irradiation once experimental data have been corrected for dilution and wall losses. This could suggest either an underestimation of the wall loss rate or a different oxidation mechanism in the case of adsorbed limonene. The first assumption has been tested by applying a wall loss rate of 0.2 hr^{-1}, i.e. a factor of 5 higher than what has been measured, without changing the observed trend for the total aerosol mass concentration. The reaction of OH with limonene has already been assumed to proceed mostly via the attack of the OH radical on the endo double bond rather than on the exo one [55] to explain the preferential formation of non-volatile products during the first reaction steps. Our results suggest that this phenomenon is even enhanced when limonene is adsorbed on TiO_2.

To the best of our knowledge, this study is the first to demonstrate the formation of organic particles during the photocatalytic degradation of VOCs. From an air treatment perspective, further experiments are required to characterize particle composition and therefore their potential impact on health.

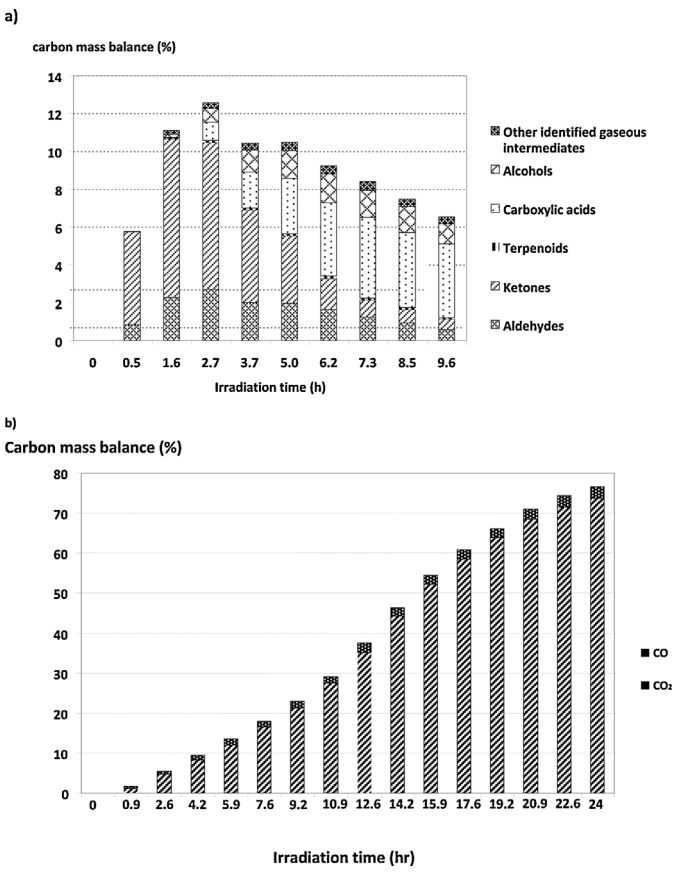

Fig. 10. Contributions of the gaseous reaction products to the carbon mass balance as a function of UV irradiation time, during the photocatalytic oxidation of 750 ppb of limonene in dry conditions: (a) organic reaction intermediates; (b) CO and CO_2.

3.3. Evolution of carbon mass balance during limonene photocatalytic oxidation at ppb levels

Since the photocatalytic oxidation of limonene is carried out in a batch reactor, the carbon mass balance of the reaction has been calculated based on the 750 ppb of limonene present in the 120 L chamber at $t = 0$, corresponding to 7500 ppb equivalent carbon and 100% of the reactor carbon mass balance.

3.3.1. Contributions of gas phase organic reaction intermediates

The simultaneous quantification of limonene removal and reaction intermediates formation makes possible the calculation of their respective contributions into the reaction carbon mass balance as a function of oxidation process advancement in order to depict the partitioning of the various species. Assuming that the amount of carbon remains constant during the experiments performed in batch mode, the contribution of each gaseous compound to the carbon mass balance of the reaction has been calculated. The contributions of the VOCs belonging to the main classes (alcohol, terpenoid, ketone, etc.) are reported in Fig. 10a for 0–9.6 h of irradiation.

The contribution of organic compounds identified and quantified in the gas phase ranges from 5.8% to 12.5% of the reaction carbon mass balance. The maximum value of 12.5% is reached after only 2.7 h of treatment. It corresponds to a massive release of aldehydes and ketones during the first steps of the oxidation process. This maximum value is higher than those obtained under similar conditions with toluene (1.5%) [38] and decane (5%) [40]. Thus, the structure of the VOC considerably influences the amounts of reaction intermediates released in the gas phase. Beyond 3.7 h of treatment, the contribution of gas phase carboxylic acids and alcohols (secondary reaction intermediates) becomes predominant. The global contribution of gas phase reaction intermediates to the carbon mass balance tends to decrease mainly because of the carbonyl compound removal. After 9.6 h of treatment, secondary reaction intermediates account for more than 75% of the total gaseous reaction intermediates. Despite their high number of carbon atoms, terpenoids monitored in the gas phase are characterized by a contribution which does not exceed 0.1% of the gaseous reaction intermediates on the whole investigated time range. This value confirms a massive adsorption of the terpenoid species all along the photocatalytic process.

3.3.2. Contributions of CO and CO_2

The contributions of CO and CO_2 to the reaction carbon mass balance have been calculated for different irradiation times ranging from 0 to 24 h of treatment and reported in Fig. 10b. Unsurprisingly, compared to CO_2, the contribution of CO in the carbon mass balance is minor; indeed, it remains lower than 3% whereas CO_2 accounts for 74% after 24 h of reaction. The continuous increase of CO and CO_2 contributions in the carbon mass balance attests that no deactivation phenomenon of the photocatalyst occurs under our experimental conditions. As a result, the massive adsorption of limonene and terpenoid intermediates on the surface does not lead to an irreversible coverage of photocatalytic reactive sites. Compared to limonene removal which occurs within 10 h, mineralization is significantly delayed and requires more than 24 h. However, the fact that 77% of the carbon mass balance is represented by CO and CO_2 attests of the good performances of the photocatalytic process to achieve complete oxidation of terpenoids.

3.3.3. Contribution of SOA

The contribution of SOA to the reaction carbon mass balance has been assessed. First, the volume of SOA formed per m^3 has been evaluated from particle counting data assuming that particles are spherical. Then, considering a density of 1.25 g cm^{-3} for SOA produced from limonene [54,55], the mass concentration of particle has been calculated. Finally, the number of carbon atoms involved in SOA per m^3 has been determined considering an average (organic matter/organic carbon) ratio of 1.6 [59–61]. These data have been used to evaluate the contribution of SOA to the carbon mass balance as a function of the photocatalytic reaction advancement from 0 to 8 h. As reported in Fig. 11, the contribution of SOA in the carbon mass balance never exceeds 2%. In spite of the fact that the evaluation of SOA contribution relies on several hypotheses, it clearly appears that their contribution is one order of magnitude lower than organic gaseous intermediates. The contribution of SOA in the carbon mass balance continuously increases from 0 to 6 h and then remains constant.

3.3.4. Carbon mass balance overview

Fig. 12 gives an overview of the reaction carbon mass balance from 0 to 9.6 h of treatment. The respective contributions of limonene, gaseous reaction intermediates, particulate matter, CO and CO_2 are plotted. The contribution of particulate matter in the carbon mass balance of a photocatalytic oxidation process is assessed for the first time. After 9.6 h of batch treatment, more than 90% of limonene is removed from the gas phase. However, only 40% of the carbon balance is characterized and 60% remains unidentified. Considering the diversity and the performances of the analytical techniques used in this study, we can assume that the unidentified fraction at 9.6 h can mainly be attributed to the species adsorbed on the photocatalyst. This hypothesis is based on (i) the DRIFTS experiments and (ii) the recovery of more than 77% of the carbon balance through CO and CO_2 after 24 h of irradiation.

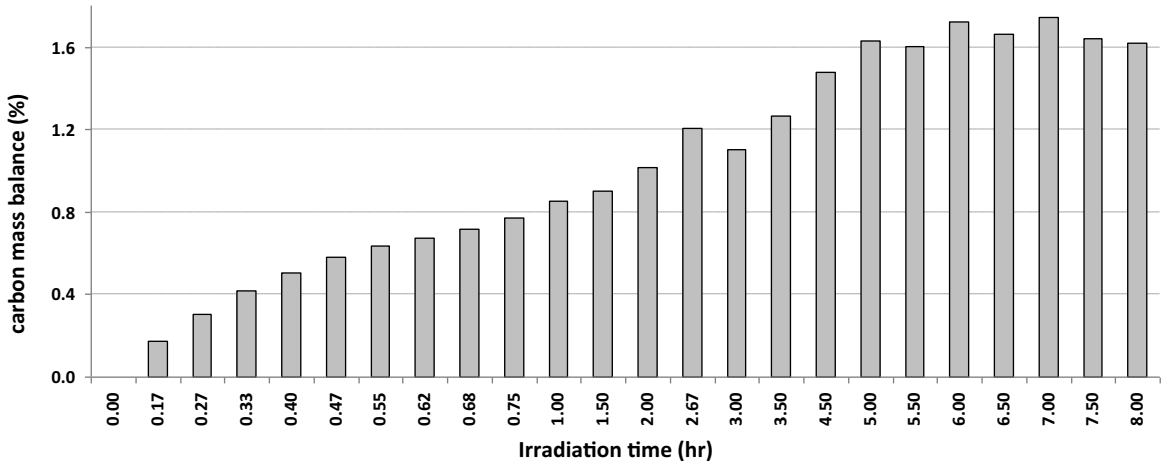

Fig. 11. Evaluation of the contribution of detected SOA to the carbon mass balance as a function of UV irradiation time, during the photocatalytic oxidation of 750 ppb of limonene in dry conditions.

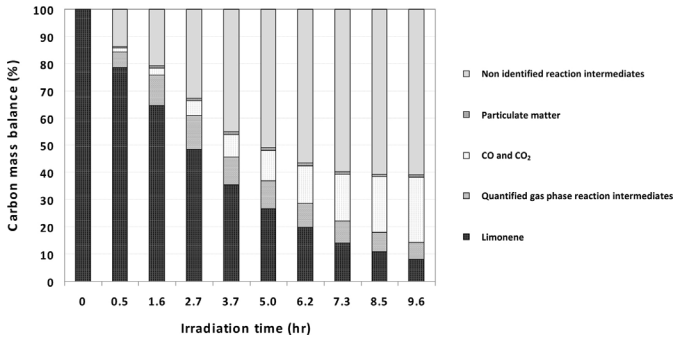

Fig. 12. Respective contributions of limonene, identified gaseous reaction intermediates, CO, CO_2, particulate matter and non-identified reaction intermediates into the carbon mass balance of 750 ppb limonene photocatalytic oxidation in dry conditions.

4. Conclusion

The photocatalytic oxidation of limonene at ppb levels has been investigated from different and complementary points of view. First, a complete characterization of the gas phase was performed by the monitoring of reaction intermediates, CO and CO_2 as a function of treatment time. Then, the identification of adsorbed phase by-products has been successfully performed using an infrared in situ monitoring of the photocatalyst surface. Finally, the formation of particulate by-products was investigated for the first time in this paper.

The results showed that heterogeneous treatment of limonene by photocatalysis follows a pseudo first order kinetics for an initial concentration of 750 ppb. A total of 20 VOCs have been identified and quantified in the gas phase. Acetone and acetaldehyde are the most abundant gaseous reaction intermediates. As soon as limonene is removed from the gas phase, those compounds disappeared. Moreover the quantity of formaldehyde remains low throughout the oxidation process.

The implementation of appropriate techniques such as DRIFT spectroscopy enabled to identify the increasing population of carbonyls, formates and alkenes as adsorbed species during UV irradiation. Although the DRIFT method used in this study did not allow quantifying the oxidized species, carbon mass balance calculations based on the quantified intermediates evidence that their abundance in the carbon balance is significant (more than 60%) after 10 h of photocatalytic treatment.

Similarly to ozonolysis and photooxidation reactions, the photocatalytic oxidation of limonene leads to the fast, but not instantaneous, formation of secondary organic aerosol, confirming that they originate from the gas-particle conversion of reaction intermediates formed during the photocatalytic process. From an indoor air quality point of view, it is important to notice that it is the lowest contribution to the carbon mass balance among the quantified reaction intermediates. However, the photocatalytically produced particles are characterized by submicron diameters and high oxygen content. As a consequence they may deeply penetrate lungs and be easily metabolized. The observation of ultrafine particles promotes the implementation of appropriate air treatment systems such as filters to avoid their release into indoor atmosphere. Limonene could be considered as a model pollutant to follow the formation of SOA in the field of air treatment by photocatalysis. Further investigations with other biogenic hydrocarbons would be interesting in order to assess their behavior in photocatalytic air treatment systems.

Acknowledgments

This work is part of the CaPPA project (Chemical and Physical Properties of the Atmosphere), funded by the French National Research Agency (ANR) through the PIA (Program d'Investissements d'Avenir) under contract ANR-10-LABX-005.

References

[1] N.E. Klepeis, W.C. Nelson, W.R. Ott, J.P. Robinson, A.M. Tsang, P. Switzer, J.V. Behar, S.C. Hern, W.H. Engelmann, J. Expo. Anal. Environ. Epidemiol. 11 (2001) 231–252.
[2] O. World Health, Environ. Technol. Lett. 10 (1989) 855–858.
[3] S.H. Shin, W.K. Jo, Chemosphere 89 (2012) 569–578.
[4] S. Kirchner, J.-F. Arenes, C. Cochet, M. Derbez, C. Duboudin, P. Elias, A. Gregoire, B. Jédor, J.-P. Lucas, N. Pasquier, Environ. Risques Santé 6 (2007) 259–269.
[5] D.A. Sarigiannis, S.P. Karakitsios, A. Gotti, I.L. Liakos, A. Katsoyiannis, Environ. Int. 37 (2011) 743–765.
[6] R. Kostiainen, Atmos. Environ. 29 (1995) 693–702.
[7] W.J. Fisk, A.H. Rosenfeld, Estimates of Improved Productivity and Health from Better Indoor Environments, in: INDOOR AIR -COPENHAGEN- INTERNATIONAL JOURNAL OF INDOOR AIR QUALITY AND CLIMATE, Munksgaard International Publishers, 1997, pp. 158–172.
[8] G. Curci, M. Beekmann, R. Vautard, G. Smiatek, R. Steinbrecher, J. Theloke, R. Friedrich, Atmos. Environ. 43 (2009) 1444–1455.
[9] J. Kesselmeier, M. Staudt, J. Atmos. Chem. 33 (1999) 23–88.
[10] S.K. Brown, M.R. Sim, M.J. Abramson, C.N. Gray, Indoor Air 4 (1994) 123–134.
[11] U. Schlink, M. Rehwagen, M. Damm, M. Richter, M. Borte, O. Herbarth, Atmos. Environ. 38 (2004) 1181–1190.
[12] D.A. Missia, E. Demetriou, N. Michael, E.I. Tolis, J.G. Bartzis, Atmos. Environ. 44 (2010) 4388–4395.

[13] B.C. Singer, H. Destaillats, A.T. Hodgson, W.W. Nazaroff, Indoor Air 16 (2006) 179–191.
[14] A.C. Steinemann, I.C. MacGregor, S.M. Gordon, L.G. Gallagher, A.L. Davis, D.S. Ribeiro, L.A. Wallace, Environ. Impact Assess. Rev. 31 (2011) 328–333.
[15] S. Krol, J. Namiesnik, B. Zabiegala, Sci. Total Environ. 468–469 (2014) 985–995.
[16] L.K. Jensen, A. Larsen, L. Molhave, M.K. Hansen, B. Knudsen, Health evaluation of volatile organic compounds (VOCs) emissions from wood and wood based materials, Arch Environ Health : Int. J. 56 (2001) 419–432.
[17] A.-T. Karlberg, A. Dooms-Goossens, Contact Dermat. 36 (1997) 201–206.
[18] J.B. Christensson, P. Forsström, A.-M. Wennberg, A.-T. Karlberg, M. Matura, Contact Dermat. 60 (2009) 32–40.
[19] K. Koistinen, D. Kotzias, S. Kephalopoulos, C. Schlitt, P. Carrer, M. Jantunen, S. Kirchner, J. McLaughlin, L. Mølhave, E.O. Fernandes, B. Seifert, Allergy 63 (2008) 810–819.
[20] T. Wainman, J. Zhang, C.J. Weschler, P.J. Lioy, Environ. Health Perspect. 108 (2000) 1139–1145.
[21] X. Chen, P.K. Hopke, Indoor Air 20 (2010) 320–328.
[22] J.Y. Zhang, K.E.H. Hartz, S.N. Pandis, N.M. Donahue, J. Phys. Chem. A 110 (2006) 11053–11063.
[23] M. Jaoui, E. Corse, T.E. Kleindienst, J.H. Offenberg, M. Lewandowski, E.O. Edney, Environ. Sci. Technol. 40 (2006) 3819–3828.
[24] T. Sun, Y. Wang, C. Zhang, X. Sun, W. Wang, Atmos. Environ. 45 (2011) 1725–1731.
[25] S. Leungsakul, M. Jaoui, R.M. Kamens, Environ. Sci. Technol. 39 (2005) 9583–9594.
[26] S. Langer, J. Moldanova, K. Arrhenius, E. Ljungström, L. Ekberg, Atmos. Environ. 42 (2008) 4149–4159.
[27] L. Morawska, C. He, G. Johnson, H. Guo, E. Uhde, G. Ayoko, Environ. Sci. Technol. 43 (2009) 9103–9109.
[28] S. Rossignol, C. Rio, A. Ustache, S. Fable, J. Nicolle, A. Même, B. D'Anna, M. Nicolas, E. Leoz, L. Chiappini, Atmos. Environ. 75 (2013) 196–205.
[29] M.S. Waring, J.A. Siegel, Environ. Sci. Technol. 47 (2013) 6341–6348.
[30] A. Fujishima, X. Zhang, Comptes Rendus Chim. 9 (2006) 750–760.
[31] A. El Otmani, Ph.D. Thesis, Ecole Nationale Supérieur de Chimie de Montpellier, 1993.
[32] I. Catanzaro, G. Avellone, G. Marci, M. Saverini, L. Scalici, G. Sciandrello, L. Palmisano, J. Hazard. Mater. 185 (2011) 591–597.
[33] M. Saverini, I. Catanzaro, G. Sciandrello, G. Avellone, S. Indelicato, G. Marci, L. Palmisano, J. Photochem. Photobiol. B: Biol. 108 (2012) 8–15.
[34] S. Poncet-Vincent, Ph.D. Thesis, Université Claude Bernard, Lyon, 1999.
[35] K.-P. Yu, G.W.-M. Lee, G.-H. Huang, J. Air Waste Manag. Assoc. (2012) 820–829, Taylor & Francis.
[36] B. Sanchez, M. Sanchez-Munoz, M. Munoz-Vicente, G. Cobas, R. Portela, S. Suarez, A.E. Gonzalez, N. Rodriguez, R. Amils, Chemosphere 87 (2012) 625–630.
[37] D. Kibanova, M. Trejo, H. Destaillats, J. Cervini-Silva, Appl. Clay Sci. 42 (2009) 563–568.
[38] O. Debono, F. Thévenet, P. Gravejat, V. Héquet, C. Raillard, L. Lecoq, N. Locoge, Appl. Catal. B: Environ. 106 (2011) 600–608.
[39] P. Coddeville, N. Locoge, J. Galloo, MERA Report, September, 1998.
[40] O. Debono, F. Thévenet, P. Gravejat, V. Héquet, C. Raillard, L. Le Coq, N. Locoge, J. Photochem. Photobiol. A: Chem. 258 (2013) 17–29.
[41] F. Thevenet, C. Guillard, A. Rousseau, Chem. Eng. J. 244 (2014) 50–58.
[42] P. Oliveira, M.L. Rojas-Cervantes, A.M. Ramos, I.M. Fonseca, A.M.B. do Rego, J. Vital Catal. Today 118 (2006) 307–314.
[43] V. Kutty, R.J. Braddock, G.D. Sadler, J. Food Sci. 59 (1994) 402–405.
[44] C. Sell, A Fragrant Introduction to Terpenoid Chemistry, Royal Society of Chemistry, 2003.
[45] K.E. Andersen, Contact Dermat. 4 (1978) 195–198.
[46] E. Paulsen, K.E. Andersen, L. Carsen, H. Egsgaard, Contact Dermat. 29 (1993) 138–143.
[47] A.-T. Karlberg, A. Boman, B. Melin, Ann. Occup. Hyg. 35 (1991) 419–426.
[48] J. Rasko, J. Kiss, Appl. Catal. A: Gen. 287 (2005) 252–260.
[49] J.M. Coronado, S. Kataoka, I. Tejedor-Tejedor, M.A. Anderson, J. Catal. 219 (2003) 219–230.
[50] B. Stuart, Infrared Spectroscopy, Wiley Online Library, 2004.
[51] I. Salem, N. Keller, V. Keller, Green Chem. 11 (2009) 966–973.
[52] R.M. Alberici, W.F. Jardim, Appl. Catal. B: Environ. 14 (1997) 55–68.
[53] A. Calogirou, B. Larsen, D. Kotzias, Atmos. Environ. 33 (1999) 1423–1439.
[54] H. Kim, S.E. Paulson, Atmos. Chem. Phys. 13 (2013) 7711–7723.
[55] N.L. Ng, J.H. Kroll, M.D. Keywood, R. Bahreini, V. Varutbangkul, R.C. Flagan, J.H. Seinfeld, A. Lee, A.H. Goldstein, Environ. Sci. Technol. 40 (2006) 2283–2297.
[56] R.K. Pathak, C.O. Stanier, N.M. Donahue, S.N. Pandis, J. Geophys. Res.: Atmos. 112 (2007) D03201.
[57] A.A. Presto, N.M. Donahue, Environ. Sci. Technol. 40 (2006) 3536–3543.
[58] C. Coeur-Tourneur, A. Tomas, A. Guilloteau, F. Henry, F. Ledoux, N. Visez, V. Riffault, J.C. Wenger, Y. Bedjanian, Atmos. Environ. 43 (2009) 2360–2365.
[59] M. Kalberer, D. Paulsen, M. Sax, M. Steinbacher, J. Dommen, A. Prevot, R. Fisseha, E. Weingartner, V. Frankevich, R. Zenobi, Science 303 (2004) 1659–1662.
[60] Y. Pang, B. Turpin, L. Gundel, Aerosol Sci. Technol. 40 (2006) 128–133.
[61] A.P. Bateman, S.A. Nizkorodov, J. Laskin, A. Laskin, Phys. Chem. Chem. Phys. 11 (2009) 7931–7942.